Document Version:

This is the Accepted Manuscript version.
The version in the University of Hertfordshire Research Archive may differ from the final published version.

Enquiries

If you believe this document infringes copyright, please contact the Research & Scholarly Communications Team at rsc@herts.ac.uk

A novel hybrid energy system combined with solar-road and soil- regenerator: Dynamic model and operational performance

Bo Xiang[a], Xiaoling Cao[a], Yanping Yuan[a,*], Liangliang Sun[a], Hongwei Wu[b], Fariborz Haghighat[c]

[a] School of Mechanical Engineering, Southwest Jiaotong University, Chengdu 610031, Sichuan, China
[b] School of Engineering and Technology, University of Hertfordshire, Hatfield AL10 9AB, United Kingdom
[c] Department of Building, Civil and Environmental Engineering, Concordia University, Montreal H3G 1M8, Canada

ABSTRACT

Solar roads are emergent and huge energy source in traffic domains. To improve the energy utilization efficiency of a solar road, a novel solar-road and soil-regenerator hybrid energy system in combination with conventional photovoltaic-thermal and soil heat storage technology was proposed. A mathematical model of the solar-road and soil-regenerator hybrid energy system was developed, validated, and applied to evaluate the thermal storage and power generation performance of the proposed system in cold regions. The results indicated that for critical thermal storage temperatures of 20, 30, and 40 °C, the proposed system decreased maximum photovoltaic cell temperatures by 24.09, 25.84, and 24.42 °C and increased electrical efficiencies by 6.85, 6.68, and 4.53%, respectively, compared with conventional solar roads. By storing heat in the soil and elevating soil temperatures, the proposed system also increased the average borehole wall temperatures by 2.93, 2.26, 1.87 °C. The proposed system produced overall energy efficiencies of 48.42, 55.47, and 66.58%, while conventional solar road efficiencies approximate 10.75%.

1. Introduction

Energy is important for economic and social development. Fossil-fuel-based energy shortages and environmental pollution have spurred interest in solar energy as a promising renewable energy source [1]. Solar energy must be captured, converted, and stored in a cost-effective fashion to promote the application [2]. Nowadays, primary methods of capturing solar energy include photovoltaic (PV) and thermal processes [3]. Solar energy is gradually applied to transportation sector with the development of solar energy utilization technology. Efthymiou et al. [4] investigated the impact of PV pavements in the urban environment. Nasir et al. [5] expanded the investigation of the road pavement solar collector system based on four tested parameters. Literature [6] reported that the Italy government is getting ready to begin construction on what is to be the world's first totally solar highway. Literature [7] reported that solar panels produce energy for high-speed trains.

First proposed by Scott Brusaw, an American engineer, solar roads have garnered interest recently [8]. A solar road is a low-carbon, environmentally friendly alternative that supports conventional transportation functions while providing output electricity for street lights, traffic lights, and residential household electricity. In 2014, the Netherlands built the world's first solar bicycle path, and in 2016, France built the world's first solar road, *Wattway*, in Normandy [9].

Analysis of the solar bicycle path indicated a photoelectric conversion efficiency of 8.6%, which is lower than the efficiency of ordinary roof solar panels. The fixed installation angle and high operating temperature of the solar cell contribute to this reduced efficiency. The highest operating temperature measured was 85.98 °C [10]. For each 1 °C increase in solar cell temperature, electrical efficiency decreases approximately 0.5% [11].

Photovoltaic-thermal (PVT) technology, which produces electricity and heating energy simultaneously, has proven effective in maintaining solar cell efficiency [12]. The PVT technology produces heating energy temperatures of 40–60 °C, and has been applied in low-temperature heating systems [13]. Pei et al. [14] analyzed the performance of heat pipe PVT systems for domestic hot water throughout the year. Izquierdo and Agustín-Camacho [15] carried out an experimental research with a PVT micro grid feeding a reversible air–water heating capacity heat pump for radiant heated floor. Chen et al. [16] proposed a heat-pipe solar (HPS) PVT heat pump system which combined the HPS PVT

Nomenclature

PV photovoltaic
PVT photovoltaic-thermal
SRSRHES solar-road and soil-regenerator hybrid energy system

Symbols

A	solar road area [m^2]
C	specific thermal capacity [J/(kg·K)]
$d_{sr,i}$	internal diameters of pipe in solar road [m]
$d_{sr,o}$	external diameters of pipe in solar road [m]
G	solar irradiance [W/m^2]
H	borehole depth [m]
h_c	convective heat transfer coefficient [W/(m^2·K)]
h_o	convective heat transfer coefficient between the outside and the transparent [W/(m^2·K)]
h_r	radiation heat transfer coefficient [W/(m^2·K)]
$h_{sr,f}$	heat transfer coefficient from pipe in solar road to fluid [W/(m^2·K)]
l	thickness [m]
Q_e	electric energy production [J]
Q_{th}	heat storage capacity [J]
q_1	heat flow between the left pipe and the borehole per microelement [W/m]
q_2	heat flow between the right pipe and the borehole per microelement [W/m]
q_{12}	heat flow between the left and right pipe per microelement [W/m]
R	thermal conductive resistance [K/W]
Ra	Rayleigh number
R_1^{Δ}	thermal resistance between the left pipe and borehole [K/W]
R_2^{Δ}	thermal resistance between the right pipe and borehole [K/W]
R_{12}^{Δ}	thermal resistance between the adjacent pipes [K/W]
S	source term
T	temperature [°C]
T_{f1}	fluid temperature in the left leg [°C]
T_{f2}	fluid temperature in the right leg [°C]
T_{st}	Critical thermal storage temperatures [°C]
t	time [s]
V	flow rate [m/s]

v_r	wind speed [m/s]
M	mass fluid flow [kg/s]
w	width [m]
x,y,z	Cartesian coordinates

Greek symbols

α	absorptivity
β	title angle [°]
o	Stefan-Boltzmann constant [W/(m^2·K^4)]
ε	emittance
η_e	electrical efficiency of proposed system
η_f	primary energy-saving efficiency
η_p	electric power generation efficiency of conventional power plant
η_{pv}	electrical efficiency of PV cell
η_r	reference energy efficiency of PV cell
η_{th}	thermal storage of proposed system
η_t	overall energy efficiency
λ	thermal conductivity [W/(m·K)]
ρ	density [kg/m^3]
τ	transmissivity

Subscripts

a	air
c	thermal absorber
g	ground
in	isolating layer
B	bond
b	borehole wall
oa	outdoor air
p	photovoltaic cell
si	silicone gel
so	soil
sr,f	fluid in solar road's pipe
t	transparent surface
tw	pipe wall
U-in	inlet fluid of U-pipe
U-out	outlet fluid of U-pipe

collector with heat pump. The authors investigated the performance of the system with numerical and experimental method. Systems using PVT technology have demonstrated efficiencies of 60–80% [17].

To compensate for the seasonal dispersion and instability of solar energy, energy produced in the summer must be stored and used to supplement the winter heat demand, especially in cold regions [18]. The shallow stratigraphic soil supporting a solar road, with good heat storage properties, may serve as a regenerator [19]. The ground heat exchanger (GHE) is an advisable design for storing heat in soil. Cao et al. [20] developed a heat transfer model of the GHE by combining the analytical solution and numerical solution, and investigated on the restoration performance of vertical ground heat exchanger with various intermittent ratios. Yuan et al. [21] investigated the thermal interaction of multiple boreholes, the soil hear transfer properties of a large soil area is the focus.

Moreover, some studies have considered solar energy-soil thermal storage using a combination of solar energy technology and ground source heat pump systems [22]. Liu et al. [23] designed and implemented an experiment of solar seasonal storage coupling with ground-source heat pump system. Aim at this system, thermal equilibrium of soil was studied; relationship between solar energy radiation quantity and thermal storage quantity was discussed. Results showed that solar energy utilization efficiency achieved 50.2% and soil temperature raised by 0.21 °C. Wang et al. [24] studied a solar-assisted ground-coupled heat pump system with solar seasonal thermal storage installed in a detached house in Harbin using experimental method. The results show that the system can meet the heating–cooling energy needs of the building. The average coefficient of performance (COP) of the system was 6.55 in winter and that was 21.35 in summer, and the heat directly supplied by solar collectors accounted for 49.7% of the total heating output in winter. After a year of operation, the heat extracted from the soil by the heat pump accounted for 75.5% of the heat stored by solar seasonal thermal storage. Dai et al. [25] empirically investigated the effects of operation mode on the heating performance of a solar-assisted ground source heat pump system (SAGSHPS) and found that the solar energy accelerated soil temperature recovery when the heat pump system was not operational. In addition, the solar energy storage time was optimized to reduce the energy consumption of the circulating water pump according to storage tank temperature. Chen and Yang [26] used the Transient System Simulation Tool (TRNSYS) to

determine the performance of a SAGSHPS under different weather conditions and optimize the solar collector area and buried pipe lengths. Using the optimum collector area of 40 m² and buried pipe length of 264 m under a determined load, the SAGSHPS was estimated to satisfy 75% of the annual heat demand. Moreover, the energy balance of the optimized design was confirmed with a minor difference of 0.75%. Alternatively, Zhang et al. [27] proposed a seasonal solar soil heat storage system (SSSHSS) for greenhouse heating that accounted for the summer supply/winter demand imbalance and offered lower operating costs than traditional geothermal systems because it does not require a heat pump. Compared with conventional solar heating systems, the SSSHSS produced an annual energy savings in Shanghai of 27.8 kWh/m² with a minimum year-round indoor greenhouse air temperature of 12 °C. Meanwhile, some researchers use pavement as cover of solar collector [28]. Ozgener [29] studied the performance characteristics of a solar assisted ground-source heat pump system (drive way used as solar collector) for greenhouse heating. It found that the exergy efficiency value for the whole system reached 68%.

Building upon these earlier studies, in order to make full use of solar energy throughout the year, and taking into account the advantages of PVT and soil heat storage, thus, a novel solar-road and soil-regenerator hybrid energy system (SRSRHES) used in combination with conventional PVT and soil heat storage technology was proposed. A mathematical model of the SRSRHES was developed, validated, and used in cold regions to determine the thermal storage and power generation performance of the proposed system. In this paper, three operating modes that critical thermal storage temperatures of 20, 30, and 40 °C was simulated with above mathematical model, and the PV temperature, borehole wall temperature, electric energy production, heat storage capacity and energy efficiency were analyzed to evaluate the performance of the proposed system when applied in cold regions. The results showed these efficiencies were consistently higher than conventional solar road efficiencies (approximately 10.75%) confirming

the merit of the proposed SRSRHES in solar road applications. The observed benefits of conventional PVT and soil heat storage technologies in this type of application were consistent with prior study results, and the proposed SRSRHES further enhanced these benefits.

2. Proposed hybrid energy system combined with solar-road and soil-regenerator

A conventional solar road comprises an isolating layer, PV cells, and a transparent surface placed sequentially on the original subgrade. Fig. 1a shows a schematic of a conventional solar road. The isolating layer prevents moisture from the soil from reaching the internal components, the PV cells generate power, and the transparent surface further protects the internal components while allowing the transmission of sunlight.

The SRSRHES proposed in this study is based on a typical conventional solar road design but includes a soil regenerator and accumulator. Fig. 1b and c show standard and magnified scale schematics of the proposed SRSRHES. The SRSRHES includes an isolating layer, pipes, a thermal absorber, PV cells, and a transparent surface placed sequentially on the original subgrade. While supporting its basic transportation functions, the solar road concurrently converts solar energy to heat and electricity. The supplemental soil regenerator and coupled soil-ground heat exchanger provide heat storage and release. The pipes in the solar road are connected to the GHE. The accumulator stores electricity generated by the solar road and provides electricity for nearby consumers.

The working principle of the SRSRHES follows. On sunny days, sunlight passes through the transparent surface and is absorbed by the PV cells. A portion of the electricity generated by the PV cells is used to drive the circulating pump; the remainder is stored in the accumulator. Concurrently, the fluid in the pipes absorbs heat and is subsequently pumped to the GHE. The soil then absorbs the heat and cools the fluid.
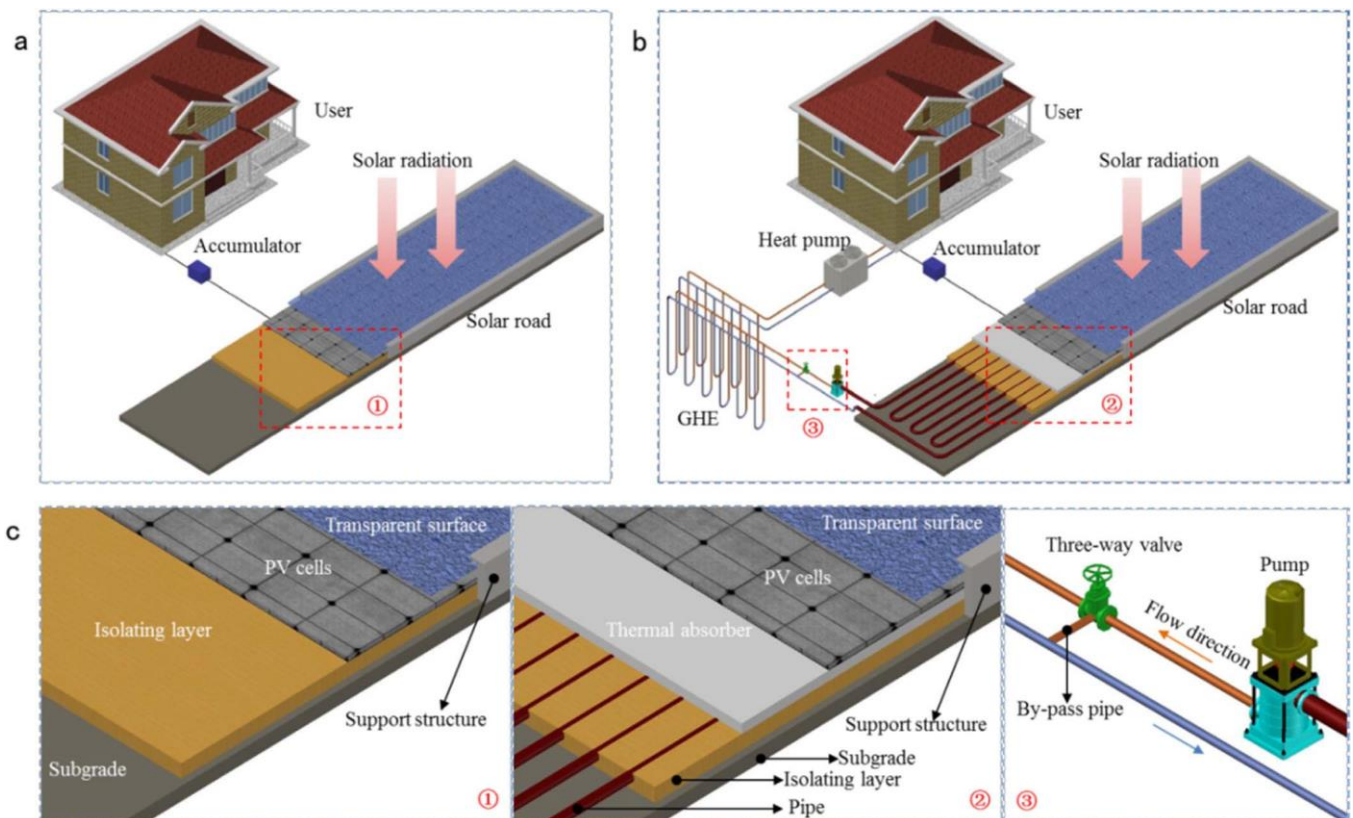

Fig. 1. Conventional solar road and proposed SRSRHES schematics: (a) conventional solar road; (b) proposed SRSRHES; (c) magnified view of proposed SRSRHES.

The cooled fluid is pumped back into the solar road's pipes to reabsorb heat, contributing to both waste heat recovery and heat storage.

When the system is operational, if the outlet temperature reaches the predefined critical thermal storage temperature, T_{st}, the heated fluid is directed through the GHE. If the outlet temperature does not reach the T_{st}, the heated fluid is returned to the solar road through the bypass pipe where it continues to be heated. During cold winters, the heat stored in the soil could be extracted by ground source heat pump systems and used for road snow melting or domestic heating and hot water systems.

Both conventional solar roads and the proposed SRSRHES support basic transportation functions while producing electricity. The proposed SRSRHES would uniquely increase photoelectric conversion efficiency by reducing PV cell temperatures, enhance solar energy seasonal storage, and increase the comprehensive solar energy utilization rate.

3. Mathematical model of hybrid energy system combined with solar-road and soil-regenerator

The performance of the proposed SRSRHES is affected by both the solar road and soil regenerator, which are interrelated and restrictive. As such, the mathematical model developed in this study to evaluate the performance of the SRSRHES considered the effects of the solar road and soil regenerator simultaneously. A series of prior studies considering PVT hot water and ground source heat pump systems formed the basis for this approach. In this paper, the mathematical model of SRSRHES consists of a solar road sub-model and a soil regenerator sub-model.

3.1. Solar road sub-model

A sub-model is first developed to replicate the solar road structure. Fig. 2 shows the plan and cross-sectional views of the solar road sub-model. Parallel pipes are attached evenly along the width of solar road sub-model [30].

The heat balance for each solar road layer can be expressed mathematically. For the transparent surface, the heat balance equation can be expressed as follows [30]:

$$\rho_t C_t l_t \frac{\partial T_t}{\partial t} = \alpha_t G + h_o(T_{oa} - T_t) + h_{r,t-sky}(T_{sky} - T_t) + (h_{r,p-t} + h_{c,p-t})(T_p - T_t) \tag{1}$$
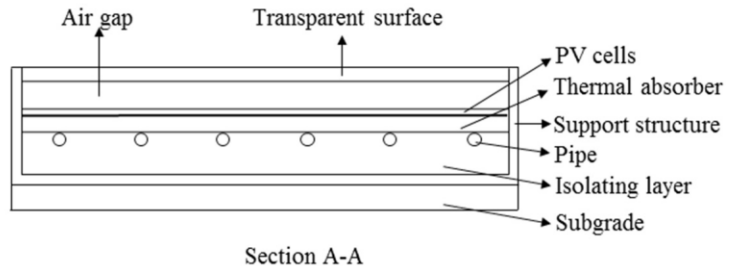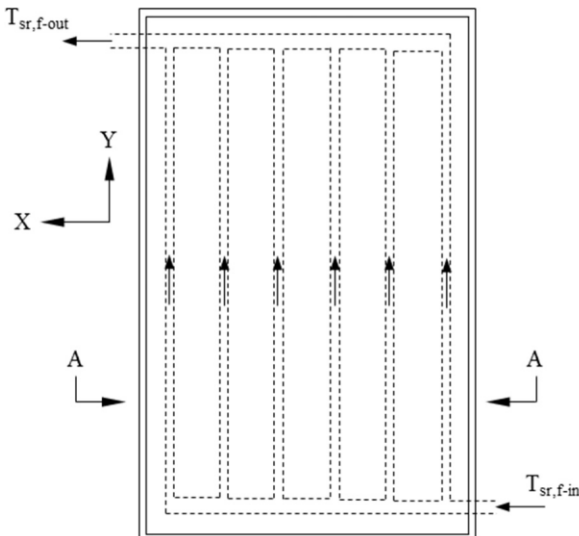
where the sky temperature is given by [33]:

$$T_{sky} = 0.0552 T_a^{1.5} \tag{2}$$

The convective heat transfer coefficient between the outside and the transparent can be expressed as follows:

$$h_o = \begin{cases} 16.21(0.68v_r - 0.5)^{0.45} & (20° \leqslant \phi \leqslant 160°) \\ 16.21(0.157v_r - 0.027)^{0.45} & (\phi \leqslant 20° \text{ or } \phi \geqslant 160°) \end{cases} \tag{3}$$

The radiation heat transfer coefficient between the sky and transparent surface can be expressed as follows:

$$h_{r,t-sky} = \sigma\varepsilon_t \frac{T_{sky}^4 - T_t^4}{T_{sky} - T_t} \tag{4}$$

The radiation heat transfer coefficient between the PV cells and the transparent surface can be expressed as follows:

$$h_{r,p-t} = \sigma \left(\frac{1}{\frac{1}{\varepsilon_p} + \frac{1}{\varepsilon_t} - 1} \right)(T_p - T_t) \tag{5}$$

The convective heat transfer coefficient between the PV cells and the transparent surface can be expressed as follows:

$$h_{c,p-t} = \frac{\lambda_a}{l_a}\left[1 + 1.44\left(1 - \frac{1708}{Ra\cdot\cos\beta}\right)^+\left(1 - \frac{1708(\sin 1.8\beta)^{1.6}}{Ra\cdot\cos\beta}\right) + \left(\left(\frac{Ra\cdot\cos\beta}{5830}\right)^{\frac{1}{3}} - 1\right)^+\right] \tag{6}$$

For the PV cells, the heat balance equation can be expressed as follows [31]:

$$\rho_p C_p l_p \frac{\partial T_p}{\partial t} = \lambda_p \frac{\partial^2 T_p}{\partial x^2}dx + \lambda_p \frac{\partial^2 T_p}{\partial y^2}dy + \alpha_p \tau_t G(1 - \eta_{pv}) + (h_{c,p-t} + h_{r,p-t})(T_t - T_p) + \frac{T_c - T_p}{R_{si}} \tag{7}$$

where the electrical efficiency of the PV cells, η_{pv}, can be written as follows:

$$\eta_{pv} = \eta_r(1 - 0.0045(T_p - 298.15)) \tag{8}$$

where η_r is the reference energy efficiency of the PV cells. Under standard test conditions, $\eta_r = 16\%$.

The heat balance equation for the thermal absorber differs with and without pipes. For a thermal absorber, the heat balance equations can be expressed as follows, with and without pipes, respectively [30]:
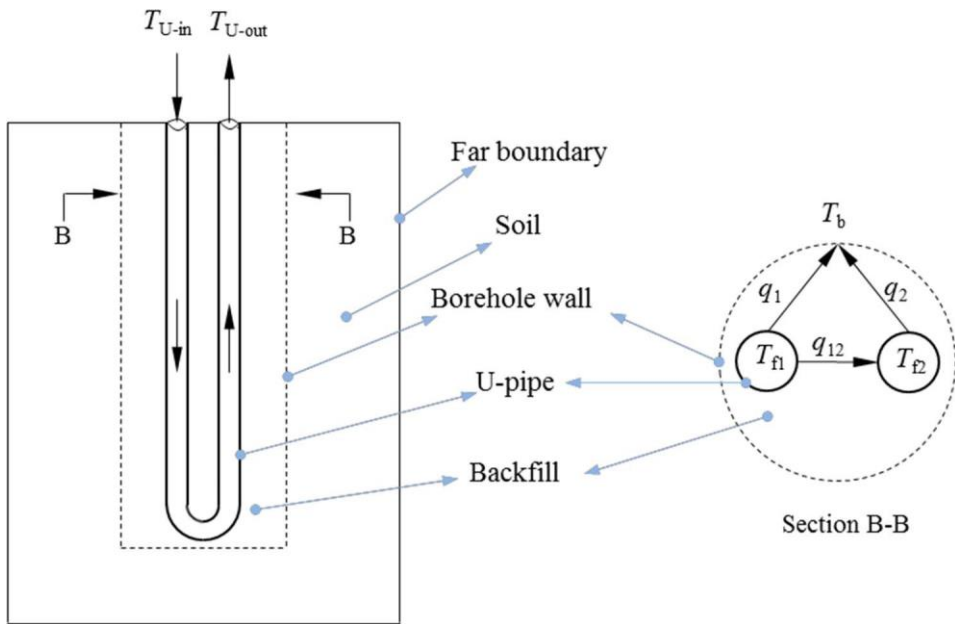

Fig. 2. Plan and cross-sectional views of the solar road sub-model.

Fig. 3. Heat transfer schematic for the soil re-generator submodel.
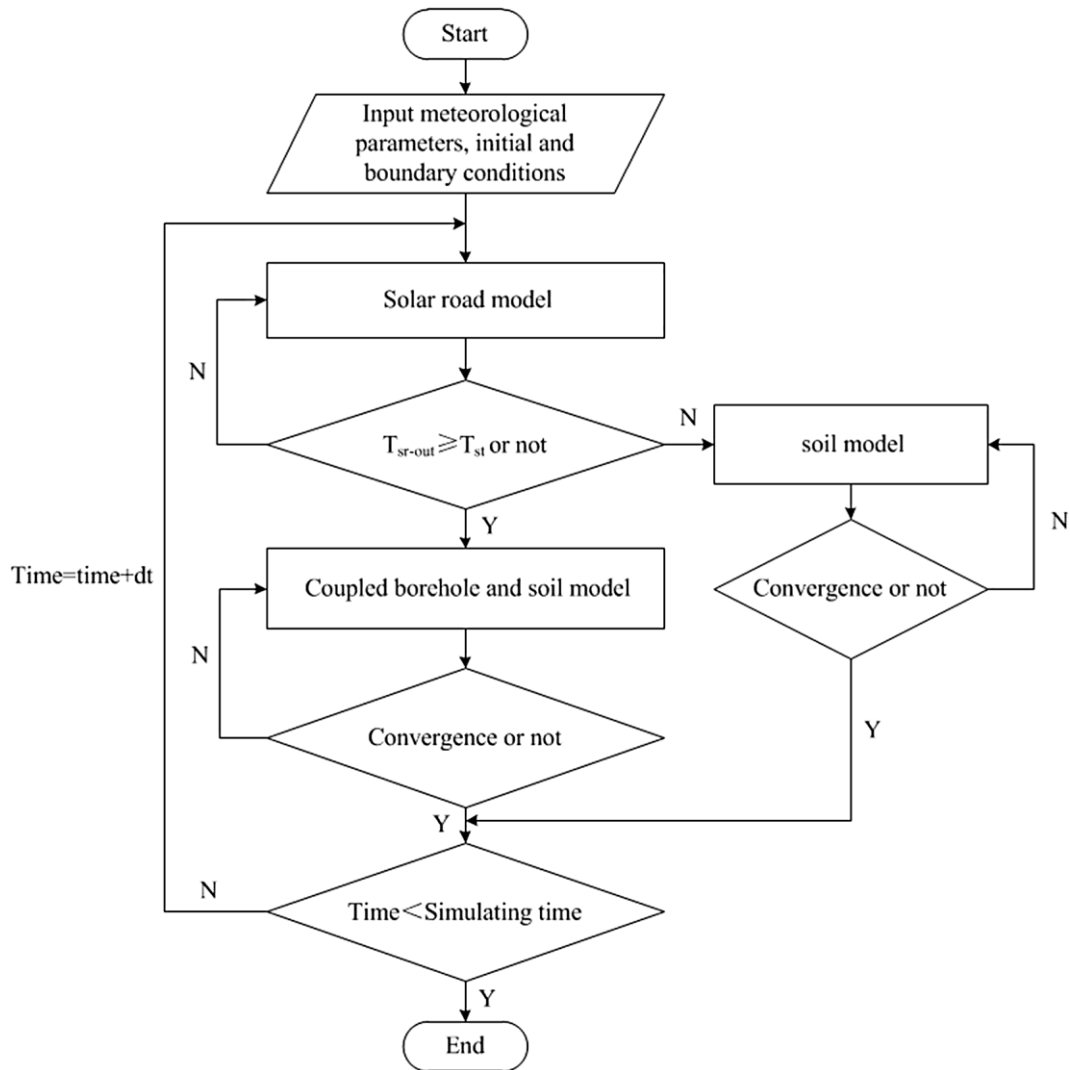
Fig. 4. Dynamic simulation process for the proposed SRSRHES.

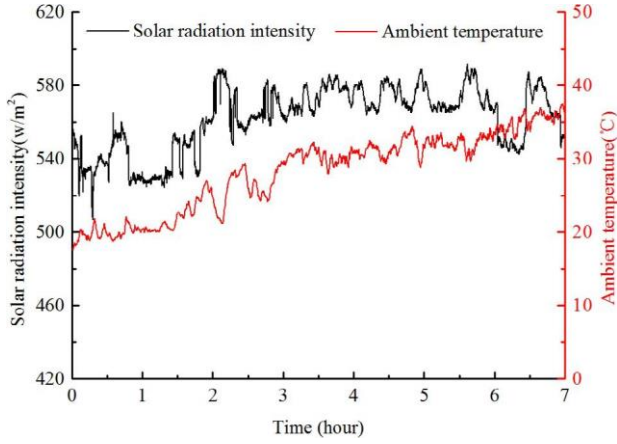| Parameter	Value
Transparent surface thickness	0.005 m
Air gap thickness	0.02 m
PV cell dimensions	1.2 m × 0.54 m × 0.006 m
Thermal absorber thickness	0.0002 m
Thermal insulation thickness	0.04 m
Thermal insulation conductivity	0.039 W/(m·K)
Internal pipe diameter	0.01 m
Number of pipes	15
Water tank dimensions	0.3 m × 0.3 m × 0.3 m

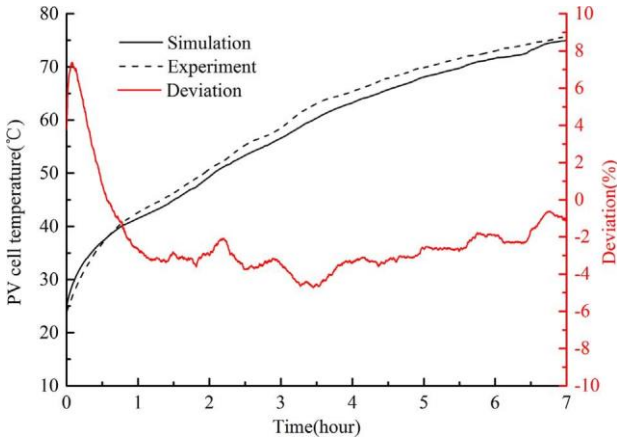Fig. 5. Meteorological parameters used for solar road sub-model validation.

Fig. 6. Comparison of experimental and simulated PV cell temperature results.

Parameter	Value
Number of boreholes	1
Borehole diameter	0.1 m
Borehole depth	1.2 m
Internal U pipe diameter	0.014 m
External U pipe diameter	0.016 m
Distances between the two pipes	0.06 m
Soil density	1322 kg/m^3
Soil specific heat	1016 J/(kg·K)
Inlet water temperature	48.6 °C
Fluid flow	0.1053 m^3/h
Soil tank dimensions	1.0 m × 1.0 m × 1.2 m
Initial soil temperature	18.9 °C

$$\rho_c C_c l_c \frac{\partial T_c}{\partial t} = \lambda_c \frac{\partial^2 T_c}{\partial x^2} \frac{dx}{2} + \lambda_c \frac{\partial^2 T_c}{\partial y^2} \frac{dy}{2} + \frac{T_p - T_c}{R_{si}}$$
$$+ \left(\frac{T_{sr,f} - T_c}{\frac{1}{h_{sr,f} \pi d_{sr,i}} + \frac{\log\left(\frac{d_{sr,o}}{d_{sr,i}}\right)}{2\pi \lambda_{tw}} + \frac{R_B}{w_B}} \right) dy \tag{9}$$

$$\rho_c C_c l_c \frac{\partial T_c}{\partial t} = \lambda_c \frac{\partial^2 T_c}{\partial x^2} \frac{dx}{2} + \lambda_c \frac{\partial^2 T_c}{\partial y^2} \frac{dy}{2} + \frac{T_p - T_c}{R_{si}} + \frac{T_g - T_c}{R_{in}} \tag{10}$$

For the fluid flow in the pipes, the heat balance equation can be expressed as follows [32]:

$$\frac{\pi d_{sr,i}^2}{4} \rho_{sr,f} C_{sr,f} \frac{\partial T_{sr,f}}{\partial t} = \frac{\pi d_{sr,i}^2}{4} \lambda_{sr,f} \frac{\partial^2 T_{sr,f}}{\partial y^2}$$
$$+ \left(\frac{T_c - T_{sr,f}}{\frac{1}{h_{sr,f} \pi d_{sr,f}} + \frac{\log\left(\frac{d_{sr,i}}{d_{sr,o}}\right)}{\frac{\pi \lambda_{tw}}{2}} + \frac{R_B}{w_B}} \right) dy$$
$$- \frac{\pi d_{sr,i}^2}{4} \rho_{sr,f} C_{sr,f} V_{sr,f} \frac{\partial T_{sr,f}}{\partial y} \tag{11}$$

where $T_{sr,f}$, $\rho_{sr,f}$, $C_{sr,f}$, and $V_{sr,f}$ are the temperature, density, thermal capacity, and flow rate of the fluid in the pipes, respectively. More detailed descriptions about the model are available in the literature [30].

3.2. Soil regenerator sub-model

Next, a sub-model to replicate the soil regenerator component was developed. In this study, a single U-shaped vertical buried pipe was used to replicate the soil regenerator. Fig. 3 shows a heat transfer schematic for the soil regenerator sub-model. Yuan et al. [21] demonstrated a method that combined numerical and analytical calculations to solve the heat transfer problem for a coupled U-shaped vertical buried pipe and soil. The calculation area was divided into two parts—the borehole area and the soil area—with the borehole as the boundary. The calculation method was analytical for the borehole area and numerical for the soil area. The two parts were coupled by the borehole wall temperature and heat flux.

The energy balance for each area can be expressed mathematically [21]. For the soil area, the energy balance equation can be expressed as follows:

$$\rho_{so} C_{so} \frac{\partial T_{so}}{\partial t} = \frac{\partial}{\partial x}\left(\lambda_{so} \frac{\partial T_{so}}{\partial x} \right) + \frac{\partial}{\partial y}\left(\lambda_{so} \frac{\partial T_{so}}{\partial y} \right) + S \tag{12}$$

where ρ_{so}, C_{so}, T_{so}, and λ_{so} are the density, thermal capacity, temperature, and thermal conductivity of the soil.

For the borehole area, the energy balance equation can be expressed as follows:

$$\begin{cases} M \frac{dT_{f1}(z)}{dz} = q_1 + q_{12} = \frac{1}{R_1^\Delta}[T_b - T_{f1}(z)] + \frac{1}{R_{12}^\Delta}[T_{f2}(z) - T_{f1}(z)] \\ -M \frac{dT_{f2}(z)}{dz} = q_2 - q_{12} = \frac{1}{R_2^\Delta}[T_b - T_{f2}(z)] - \frac{1}{R_{12}^\Delta}[T_{f2}(z) - T_{f1}(z)] \end{cases} \tag{13}$$

where M is the mass fluid flow in the pipe; $T_{f1}(z)$ and $T_{f2}(z)$ are the fluid temperatures in the left and right legs of the pipe at a depth of z m, respectively; T_b is the average temperature of borehole wall; and R_1^Δ, R_2^Δ, and R_{12}^Δ are the thermal resistances between the left pipe and borehole, the right pipe and borehole, and the adjacent pipes, respectively. If H is the borehole depth, $T_{f1}(0) = T_{U-in}$ and $T_{f1}(H) = T_{f2}(H)$. The detailed solution process of the model is available in the literature [21].

3.3. Performance evaluation

Because the proposed SRSRHES could not only produce electricity but also store heat, a performance evaluation criterion for the system should include both electrical, η_e and thermal storage, η_{th}, efficiencies
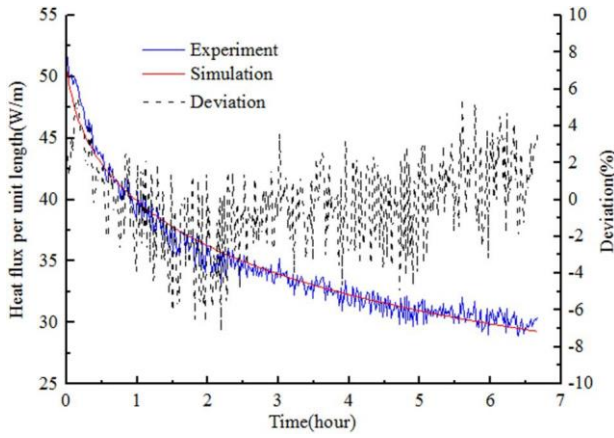
Fig. 7. Comparison of experimental and simulated heat flux per unit length results.

Table 3
SRSRHES parameters used for comprehensive model application in cold regions.

Components	Parameter	Value
Solar road	Solar road area	3 m × 10 m
	Transparent surface thickness	0.003 m
	Transparent surface emissivity	0.88
	Air gap thickness	0.02 m
	Air conductivity	0.02 W/(m·K)
	PV cell thickness	0.0005 m
	PV cell absorptivity	0.8
	PV cell transmissivity	0.9
	PV cell emissivity	0.8
	PV cell efficiency	16%
	Thermal absorber thickness	0.0005 m
	Isolating layer thickness	0.03 m
	Isolating layer conductivity	0.036 W/(m·K)
	Internal pipe diameter	0.02 m
	External pipe diameter	0.022 m
	Fluid flow in pipes	0.02 L/(m² s)
Soil regenerator	Number of boreholes	1
	Borehole diameter	0.12 m
	Borehole depth	20 m
	U pipe length	2 × 20 m
	Internal U pipe diameter	0.032 m
	External U pipe diameter	0.04 m
	Distances between the two pipes	0.025 m
	Soil density	1930 kg/m³
	Soil specific heat	1600 J/(kg·K)
	Soil thermal conductivity	2.4 W/(m·K)
	U pipe thermal conductivity	0.42 W/(m·K)
	Backfill thermal conductivity	2.6 W/(m·K)
	Initial soil temperature	10 °C

[34]. The most common evaluation criterion for system performance is the overall energy efficiency, η_t, which can be formulated as a function of η_e and η_{th} as follows:

$$\eta_t = \eta_{th} + \eta_e \tag{14}$$

While the overall energy efficiency reflects energy utilization efficiency, it does not consider energy grade differences between electricity and heat. Instead, system performance can be evaluated based on the primary energy-saving efficiency, η_f, which can be expressed as follows:

$$\eta_f = \eta_{th} + \frac{\eta_e}{\eta_p} \tag{15}$$

where η_P is the electric power generation efficiency of a conventional power plant ($\eta_P = 38\%$) and η_{th} and η_e can be calculated as follows:

$$\eta_{th} = \frac{Q_{th}}{AG} = \frac{MC_{U-in}\left(T_{U-in} - T_{U-out}\right)}{AG} \tag{16}$$

$$\eta_e = \frac{Q_e}{AG} \tag{17}$$

where Q_e and Q_{th} are electric energy production and heat storage capacity, respectively; and A is the solar road area.

3.4. Solution method of mathematical model

Eqs. (1)–(17) represent a complete mathematical description of SRSRHES performance. To evaluate the performance of the proposed SRSRHES, the solar road and GHE components were coupled by their inlet and outlet water temperatures; the inlet temperature of the GHE, T_{U-in}, was set equal to the outlet temperature of the solar road, $T_{sr,f-out}$, and the outlet temperature of the GHE, T_{U-out}, was set equal to the inlet temperature of the solar road, $T_{sr,f-in}$. To support dynamic simulation of the system, an Intel® Visual FORTRAN compiler to program the calculations was used. Fig. 4 shows the dynamic simulation process in the form of a flow chart. This process supports determination of the temperature distribution and generating capacity of the solar road, the temperature distribution and heat storage capacity of the soil, and ultimately the efficiency of the proposed SRSRHES.

4. Mathematical model validation and parameters determination

After the mathematical model for the SRSRHES was fully developed, and next the proposed model should be validated prior to application. The solar road and soil regenerator sub-models were separately validated during this process.

4.1. Solar road sub-model

Because the solar road component in this study used conventional PVT technology, it relied upon prior PVT experimental results from Ouyang et al. [31] to validate the mathematical solar road sub-model developed in this study. Ouyang et al. [31] conducted experiments using a PVT hot water system (PVT collector, water tank, and pump); solar simulator; flow meter; pyranometer; and data logger. The PVT hot water system parameters are listed in Table 1, and Fig. 5 shows the meteorological parameters used to support simulation. Fig. 6 compares a prior study's experimental and this study's simulated PV cell temperature results during a 7 h period. The unsteady operation of experimental system in the beginning, leads to PV temperature fluctuations and a larger error between the experimental and simulated results, with a maximum deviation of 7.4%. As time elapsed, the error curve flattens when the system operation becomes steady, and the errors remain within ± 5%. The high level of agreement between the experimental and simulation results suggest that the mathematical solar road sub-model developed in this study is feasible.

4.2. Soil regenerator sub-model

Similarly, the mathematical soil regenerator sub-model was validated using experimental results from Yuan et al. [21]. In this prior study, experiments were conducted for a heat transfer system using a single U-shaped vertical buried pipe. The system comprised four components: a simulated underground heat transfer system, a thermostatic water tank, a data collection system, and a pipeline loop system. A more detailed description of the system is provided by Yuan et al. [21]. Table 2 details the U pipe heat transfer system parameters used for simulation. Fig. 7 compares a prior study's experimental and this study's simulated heat flux per unit length results. The deviation between the experimental and simulated results is fluctuating and the value is –7.15% to 5.51%. The errors primarily result from the experimental system itself and from heat transfer assumptions inside the borehole. The unsteady heat transfer process inside the borehole is simplified as steady, thus leading to particular differences during
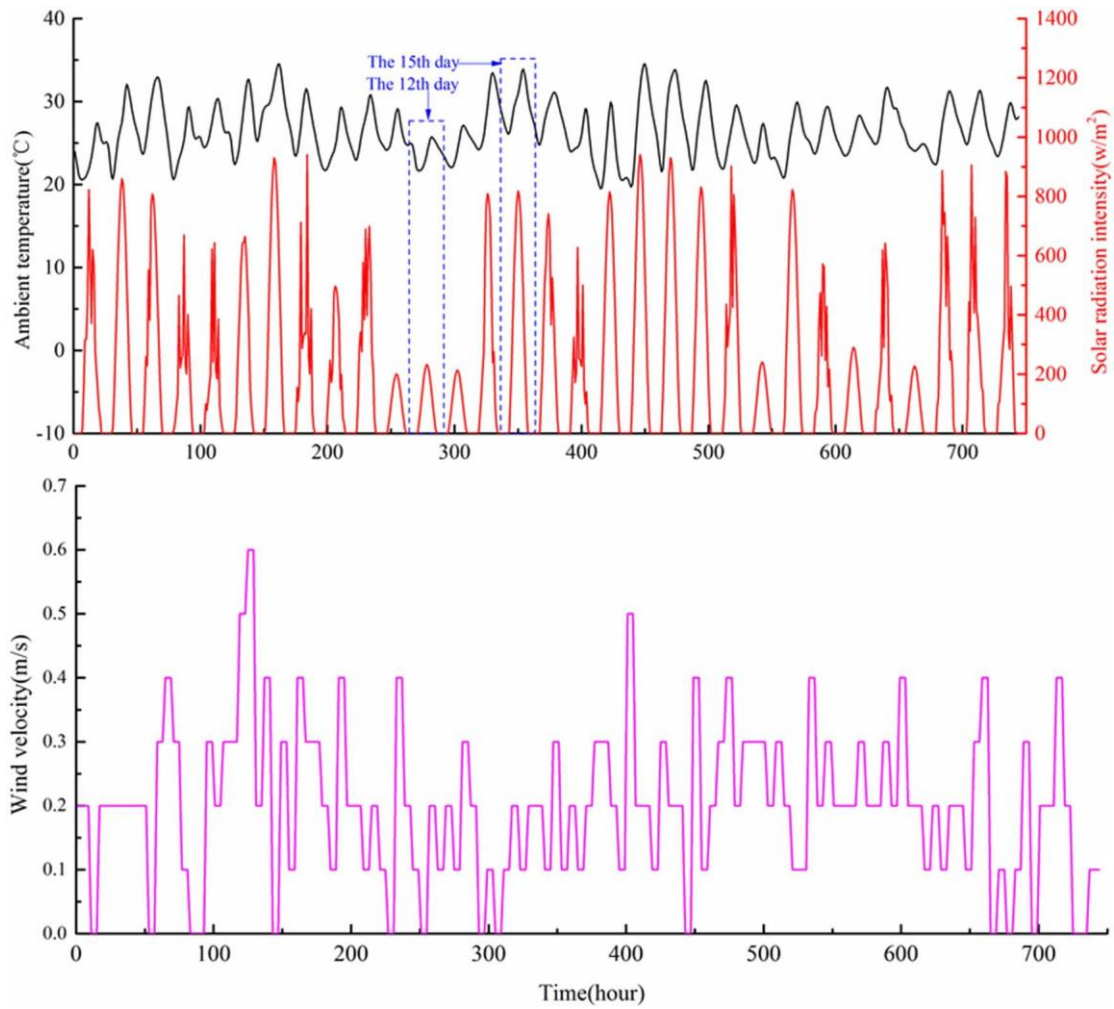
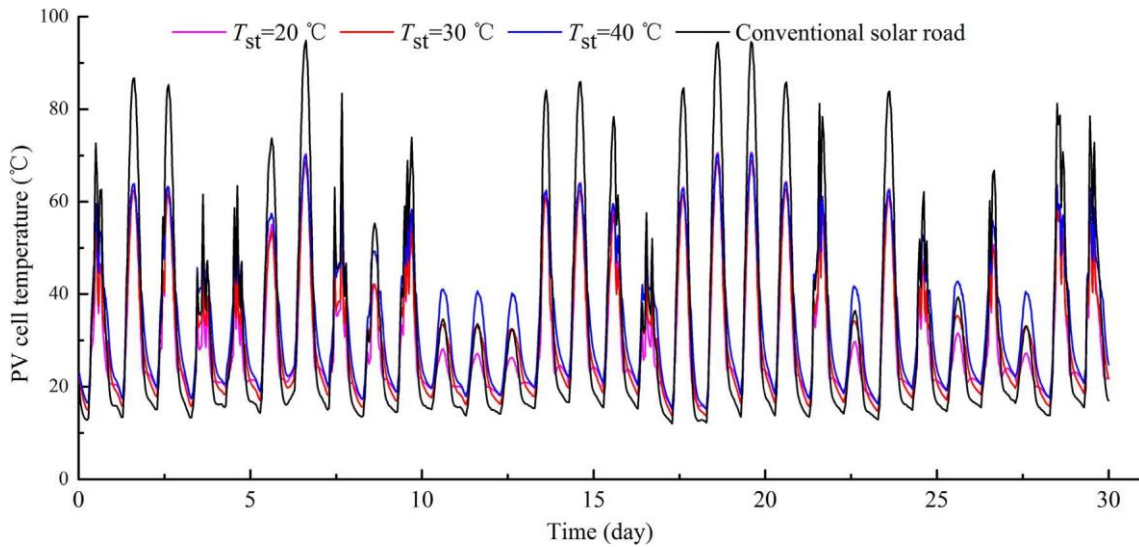Fig. 8. Meteorological parameters used in simulation.

Fig. 9. Comparison of PV cell temperatures during a typical summer month for a conventional solar road and the SRSRHES at critical thermal storage temperatures of 20, 30, and 40 °C.

operation. Again, the high level of agreement between the experimental and simulation results suggest that the mathematical soil regenerator sub-model developed in this study is feasible.

4.3. Determine main simulation parameters

After validating the individual solar road and soil regenerator sub-models, the comprehensive mathematical SRSRHES model was applied to determine the proposed system's performance in cold regions.
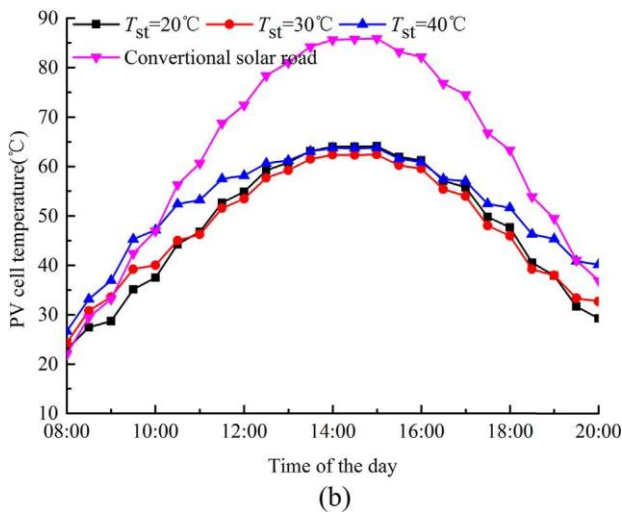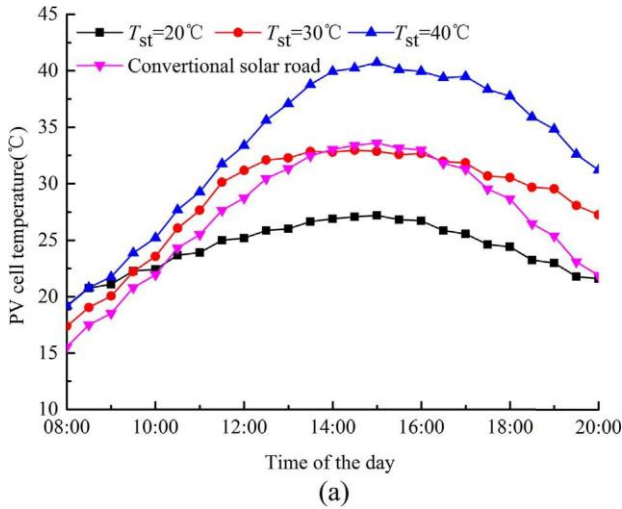
Fig. 10. Comparison of PV cell temperatures on low and high solar radiation intensity days: (a) low solar radiation intensity (12th day); (b) high solar radiation intensity (15th day).

Table 3 details the SRSRHES parameters used for comprehensive model application. The simulation reflected a typical summer month; Fig. 8 shows the meteorological parameters used, including hourly solar radiation intensity, ambient temperature, and wind velocity. Critical

thermal storage temperatures, T_{st}, of 20, 30, and 40 °C were considered.

5. Results and discussion

Based on above mentioned mathematical model, initial and boundary conditions, dynamic thermal storage performance of the system running for a month when applied in cold regions was simulated. And furthermore, the PV temperature, borehole wall temperature, electric energy production, heat storage capacity and energy efficiency were analyzed to evaluate the performance of the proposed system.

5.1. PV temperatures analysis

The PV cell temperature is an important factor that affects a solar road's photoelectric conversion efficiency. Fig. 9 compares the PV cell temperatures during a typical summer month for a conventional solar road and the SRSRHES at critical thermal storage temperatures of 20, 30, and 40 °C. In each case, the monthly PV cell temperature variation mimicked the solar radiation intensity variation. Because of the heat-removing function of its pipes, the PV cell temperatures for the SRSRHES were consistently lower than the PV cell temperatures for the conventional solar road. The maximum PV cell temperature for the conventional solar road was 94.81 °C. Comparatively, the maximum PV cell temperatures for the SRSRHES at critical thermal storage temperatures of 20, 30, and 40 °C were 70.72, 68.97, and 70.39 °C, respectively. These temperatures reflect decreases of 24.09, 25.84, and 24.42 °C, respectively, relative to the conventional solar road's maximum PV cell temperature and confirm the ability of PVT technology to reduce a solar road's PV cell temperature.

To further investigate the effects of solar radiation intensity on PV cell temperature, a low (12th day of the month) and a high (15th day of the month) solar radiation intensity days were compared. Fig. 10 shows the results of this comparison. When solar radiation intensity was low (Fig. 10a), the critical thermal storage temperature substantially affected the PV cell temperature; as the T_{st} increased, the PV cell temperatures increased. The PV cell temperature for the conventional solar road was higher than the PV cell temperature for the SRSRHES at $T_{st} = 20$ °C but lower than the PV cell temperature for the SRSRHES at $T_{st} = 30$ °C. Under low solar radiation intensity, the PV cells absorb less heat, which can be dissipated through heat exchange with the environment and road subgrade. A high critical thermal storage temperature impedes this heat dissipation, causing PV cell temperatures to increase. Therefore, a low critical thermal storage temperature is beneficial to decrease the PV cell temperature under low solar radiation
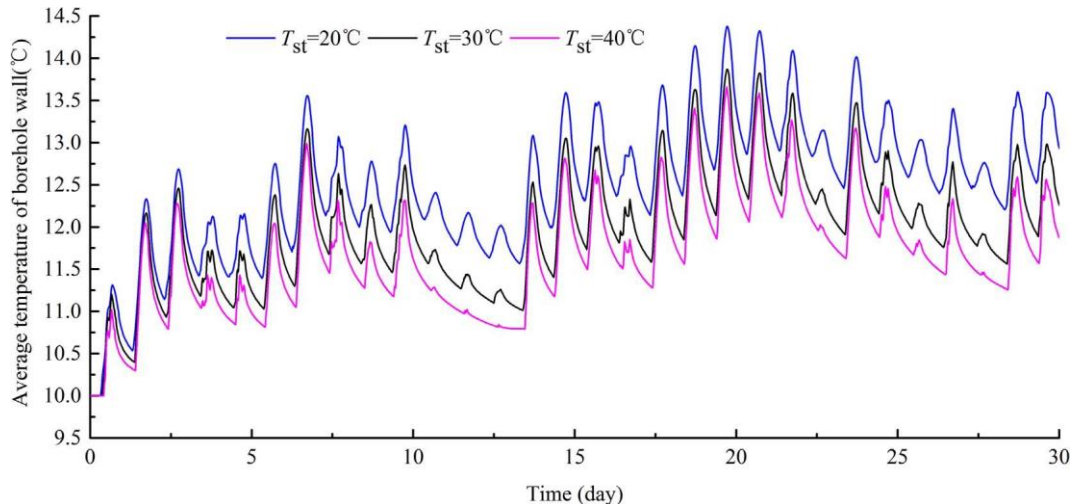

Fig. 11. Comparison of borehole wall temperatures during a typical summer month for the SRSRHES at critical thermal storage temperatures of 20, 30, and 40 °C.
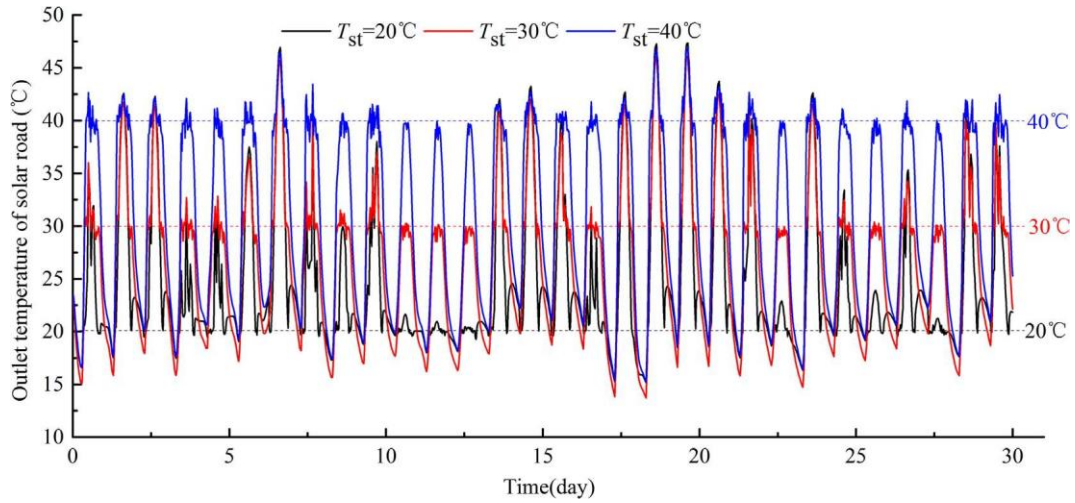
Fig. 12. Comparison of the solar road's outlet /GHE's inlet temperature during a typical summer month for the SRSRHES at critical thermal storage temperatures of 20, 30, and 40 °C.
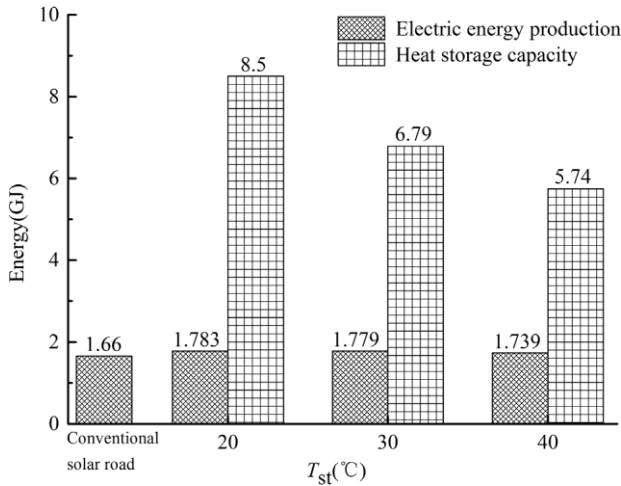

Fig. 13. Comparison of electric energy production and heat storage capacity for a conventional solar road and the SRSRHES at critical thermal storage temperatures of 20, 30, and 40 °C.
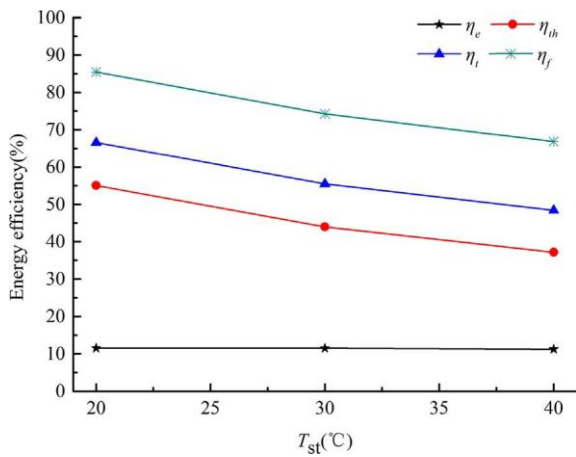

Fig. 14. Various energy efficiency parameters for the SRSRHES at critical thermal storage temperatures of 20, 30, and 40 °C.

intensity.

When the solar radiation intensity was high (Fig. 10b), the critical thermal storage temperature had a minimal effect on the PV cell temperature; as the T_{st} increased, the PV cell temperatures remained largely constant. The PV cell temperature for the conventional solar road was higher than the PV cell temperatures for the SRSRHES at each of the critical thermal storage temperatures considered, likely because of the cooling effects of the pipes. The maximum PV cell temperature for the SRSRHES at T_{st} = 40 °C was 22.17 °C lower than the maximum PV cell temperature for the conventional solar road. However, the optimal cooling effect occurred at T_{st} = 30 °C. Thus, under high solar radiation intensity, the critical heat storage temperature can be increased appropriately, increasing the heat transfer temperature difference between the fluid and the soil. Thus, an appropriate T_{st} should be determined according to different solar energy resource regions and different seasons when applied in practical engineering.

5.2. Borehole wall temperatures analysis

Fig. 11 compares the average borehole wall temperatures during a typical summer month for the SRSRHES at critical thermal storage temperatures of 20, 30, and 40 °C. The borehole wall temperatures fluctuated greatly over time, consistent with fluctuations in solar radiation intensity. During nights or days with insufficient solar radiation intensity, the system stops storing heat, and the soil temperature recovers. As the month progressed, the borehole wall temperatures trended upward. At the end of the month, the average borehole wall temperatures for the SRSRHES at critical thermal storage temperatures of 20, 30, and 40 °C were 12.93, 12.26, and 11.87 °C, respectively. These temperatures reflect increases of 2.93, 2.26, and 1.87 °C, respectively, relative to the initial temperature. From the results of literature [24], it can be seen that the soil temperatures at the depth of 30 m and 50 m increased by 4.2 °C and 3.0 °C during the process of the solar seasonal thermal storage, respectively. The temperature rise is larger than that of present work. The main reason is that the solar collector was applied to output heat only in literature [24], and it has a longer thermal storage time. If the system running time were extended, the borehole wall temperatures would continue to increase, improving the system's coefficient of performance (COP) for winter heat extraction.

As the critical thermal storage temperature decreased, the average borehole wall temperatures increased. This inverse relationship indicates that a low critical thermal storage temperature is favorable for increasing soil temperature. Under the same meteorological conditions, the outlet temperature of the solar road/inlet temperature of the GHE can more easily reach the critical thermal storage temperature when this critical temperature is low rather than high, extending the soil's effective heat storage time. Fig. 12 confirms this statement through a comparison of the solar road's outlet/GHE's inlet temperature during a

typical summer month for the SRSRHES at critical thermal storage temperatures of 20, 30, and 40 °C. As the critical thermal storage temperature increased, the amount of time that the solar road's outlet/GHE's inlet temperature exceeded the critical temperature decreased. On days with very low solar radiation intensity, such as the 12th and 13th day of the month, the solar road's outlet/GHE's inlet temperature never reached the critical thermal storage temperature of 40 °C.

The effective storage times for the SRSRHES at critical thermal storage temperatures of 20, 30, and 40 °C were 354.65, 198.65, and 126.68 h, respectively. A low critical thermal storage temperature increases the running time of the circulating water pump that drives the water flow through the GHE, and subsequently increases the corresponding energy consumption, particularly for a large-area buried pipe.

5.3. Electric energy production and heat storage capacities

Fig. 13 compares electric energy production and heat storage capacity during a typical summer month for a conventional solar road and the SRSRHES at critical thermal storage temperatures of 20, 30, and 40 °C. Electric energy productions were consistently higher for the SRSRHES than the conventional solar road; electric energy productions for the SRSRHES at critical thermal storage temperatures of 20, 30, and 40 °C were 0.123, 0.119, and 0.079 GJ higher, respectively, than the electric energy production for the conventional solar road, and the percentages increase in 7.41%, 4.17% and 4.76%, respectively. In addition, the waste heat generated by the PV cells could be recovered and stored in the soil.

The heat storage capacities for the SRSRHES at critical thermal storage temperatures of 20, 30, and 40 °C were 8.5, 6.79, and 5.74 GJ, respectively. The thermal storage powers for the SRSRHES at critical thermal storage temperatures of 20, 30, and 40 °C were 6.65, 9.49, and 12.59 kW. As the critical thermal storage temperature decreased, the average fluid-soil temperature difference decreased and the heat transfers per unit time decreased. Therefore, an appropriate critical thermal storage temperature should be selected to ensure sufficient heat storage capacity and high thermal storage power. The critical thermal storage temperature had a minimal effect on the electric energy production of the SRSRHES but had a substantial effect on its heat storage capacity. As T_{st} increased from 20 to 40 °C, the heat storage capacity decreased by 32.47%.

5.4. Energy efficiencies

Fig. 14 shows various energy efficiency parameters for the SRSRHES at critical thermal storage temperatures of 20, 30, and 40 °C. These parameters include the electrical, η_e, thermal storage, η_{th}, and overall energy, η_t, and primary energy-saving, η_f, efficiencies. The electrical efficiency had a negligible effect on the energy efficiency of the SRSRHES. The electrical efficiencies, η_e, for the SRSRHES at critical thermal storage temperatures of 20, 30, and 40 °C were 11.54, 11.52, and 11.26%, respectively. These efficiencies reflect an increase of 6.85, 6.68, and 4.53%, respectively, relative to the 10.75% electrical efficiency of the conventional solar road. The thermal storage efficiencies, η_{th}, for the SRSRHES at critical thermal storage temperatures of 20, 30, and 40 °C were 55.03, 43.96, and 37.16%, respectively. Largely dependent upon the thermal storage efficiency, the overall energy, η_t, and primary energy-saving, η_f, efficiencies for the SRSRHES at critical thermal storage temperatures of 20, 30, and 40 °C were 48.42, 55.47, and 66.58% and 66.79, 74.27, and 85.41%, respectively.

For a conventional solar road, its overall energy efficiency is equal to its electrical efficiency. As demonstrated here, the proposed SRSRHES not only improves the photoelectric conversion efficiency, but also greatly improves the utilization rate of solar energy. Moreover, this conclusion can also be obtained by comparing with the results of literature [10], which presents an 8.6% electrical efficiency of solar road and is no heat output.

6. Conclusion

To improve the energy utilization efficiency of a conventional solar road, a novel SRSRHES used in combination with conventional PVT and soil heat storage technology was proposed. This proposed system can perform its basic transportation functions, produce electricity, and store heat concurrently. In this study, a mathematical model of the SRSRHES was developed, validated, and applied in cold regions to determine the thermal storage and power generation performance of the proposed system. Results indicated that for critical thermal storage temperatures of 20, 30, and 40 °C, the SRSRHES led to a decrease in the maximum PV cell temperatures by 24.09, 25.84, and 24.42 °C and increased electrical efficiencies by 6.85, 6.68, and 4.53%, respectively, compared with conventional solar roads. By storing heat in the soil via the GHE and elevating soil temperatures, the SRSRHES also increased the average borehole wall temperatures by 2.93, 2.26, 1.87 °C. The SRSRHES produced overall energy efficiencies of 48.42, 55.47, and 66.58%; comparatively, conventional solar road efficiencies approximate 10.75%.

The results of this study substantially contribute to the state of knowledge regarding solar road designs. The research provides an enhanced theoretical understanding of thermal storage/power generation performance and the potential for direct improvements to solar-based equipment designs. Of course, there are a lot of research works that are worth being done before the proposed system applied in practical engineering. Thereby, the studies about the influence of proposed solution on the original subgrade structure and its optimization, annual operating performance of the system, optimization of system operation strategy and thermo-economic analysis should be carried out in next work.

Acknowledgements

References

[1] Ni G, Li G, Boriskina SV, Li H, Yang W, Zhang T, et al. Steam generation under one sun enabled by a floating structure with thermal concentration. Nat Energy 2016;1:16126.

[2] Lewis NS. Toward cost-effective solar energy use. Science 2007;315(5813):798–801.

[3] Kraemer D, Poudel B, Feng HP, Caylor JC, Yu B, Yan X, et al. High-performance flat-panel solar thermoelectric generators with high thermal concentration. Nat Mater 2011;10(7):532–8.

[4] Efthymiou C, Santamouris M, Kolokotsa D, Koras A. Development and testing of photovoltaic pavement for heat island mitigation. Sol Energy 2016;130:148–60.

[5] Nasir DSNM, Hughes BR, Calautit JK. A CFD analysis of several design parameters of a road pavement solar collector (RPSC) for urban application. Appl Energy 2017;186(3):436–49.

[6] Italy Prepares to Build the World's First Solar Energy Highway, < http://www.solarfeeds.com/italy-prepares-to-build-the-worlds-first-solar-energy-highway >; [accessed 17 October 2017].

[7] Jones J. NewsBriefs: solar panels produce energy for high-speed trains in europe (Discovery News). Civil Eng—ASCE 2011;81.

[8] Concept Phase, < http://www.solarroadways.com/About/Journey >; [accessed 17 June 2017].

[9] Northmore A. Canadian solar road panel design: a structural and environmental analysis. Univ Waterloo 2014:25–8.

[10] Prasanth V, Scheele N, Visser E, Shekhar A, Mouli GRC, Bauer P, et al. Green energy based inductive Self-Healing highways of the future. In: Transportation electrification conference and expo 2016;1–8.

[11] Atkin P, Farid MM. Improving the efficiency of photovoltaic cells using PCM infused graphite and aluminium fins. Sol Energy 2015;114:217–28.

[12] Zhang X, Zhao X, Smith S, Smith S, Xu J, Yu X. Review of R&D progress and practical application of the solar photovoltaic/thermal (PV/T) technologies. Renew Sust Energy Rev 2012;16(1):599–617.

[13] Wang Y, Ji J, Sun W, Yuan W, Cai J, Guo C, et al. Experiment and simulation study on the optimization of the PV direct-coupled solar water heating system. Energy 2016;100:154–66.

[14] Pei G, Fu H, Ji J, Chow TT, Zhang T. Annual analysis of heat pipe PV/T systems for domestic hot water and electricity production. Energy Convers Manage

2012;56(56):8–21.

[15] Izquierdo M, Agustín-Camacho PD. Solar heating by radiant floor: experimental results and emission reduction obtained with a micro photovoltaic–heat pump system. Appl Energy 2015;147:297–307.

[16] Chen H, Zhang L, Jie P, Xiong Y, Xu P, Zhai H. Performance study of heat-pipe solar photovoltaic/thermal heat pump system. Appl Energy 2017;190:960–80.

[17] Putrayudha SA, Kang EC, Evgueniy E, Libing Y, Lee EJ. A study of photovoltaic/thermal (PVT)-ground source heat pump hybrid system by using fuzzy logic control. Appl Therm Eng 2015;89:578–86.

[18] Reda F, Arcuri N, Loiacono P, Mazzeo D, Lund H, Kaiser MJ. Energy assessment of solar technologies coupled with a ground source heat pump system for residential energy supply in Southern European climates. Energy 2015;91:294–305.

[19] Yuan Y, Cao X, Sun L, Lei B, Yu N. Ground source heat pump system: a review of simulation in China. Renew Sust Energy Rev 2012;16(9):6814–22.

[20] Cao X, Yuan Y, Sun L, Lei B, Yu N, Yang X. Restoration performance of vertical ground heat exchanger with various intermittent ratios. Geothermics 2015;54:115–21.

[21] Yuan Y, Cao X, Wang J, Sun L. Thermal interaction of multiple ground heat exchangers under different intermittent ratio and separation distance. Appl Therm Eng 2016;108:277–86.

[22] Si Q, Okumiya M, Zhang X. Performance evaluation and optimization of a novel solar-ground source heat pump system. Energy Build 2014;70(70):237–45.

[23] Liu L, Zhu N, Zhao J. Thermal equilibrium research of solar seasonal storage system coupling with ground-source heat pump. Energy 2016;99:83–90.

[24] Wang X, Zheng M, Zhang W, Zhang S, Yang T. Experimental study of a solar-assisted ground-coupled heat pump system with solar seasonal thermal storage in severe cold areas. Energy Build 2010;42(11):2104–10.

[25] Dai L, Li S, Lin DM, Li X, Shang Y, Dong M. Experimental performance analysis of a solar assisted ground source heat pump system under different heating operation modes. Appl Therm Eng 2015;75(75):325–33.

[26] Xi C, Yang H. Performance analysis of a proposed solar assisted ground coupled heat pump system. Appl Energy 2012;97(9):888–96.

[27] Zhang L, Xu P, Mao J, Tang X, Li Z, Shi J. A low cost seasonal solar soil heat storage system for greenhouse heating: design and pilot study. Appl Energy 2015;156:213–22.

[28] Nasir DSNM, Hughes BR, Calautit JK, Lund H, Kaiser MJ. A study of the impact of building geometry on the thermal performance of road pavement solar collectors. Energy 2015;93(2):2614–30.

[29] Ozgener O, Ozgener L. Modeling of driveway as a solar collector for improving efficiency of solar assisted geothermal heat pump system: a case study. Renew Sust Energy Rev 2015;46:210–7.

[30] Sun L, Li M, Yuan Y, Cao X, Lei B, Yu N. Effect of tilt angle and connection mode of PVT modules on the energy efficiency of a hot water system for high-rise residential buildings. Renew Energy 2016;93:291–301.

[31] Ouyang L, Sun L, Yuan Y, Cao X, Xiang B. Optimum connection modes for photovoltaic thermal collectors in different radiation zones of China. Appl Therm Eng 2017;122:661–72.

[32] Yuan Y, Ouyang L, Sun L, Cao X, Xiang B, Zhang X. Effect of connection mode and mass flux on the energy output of a PVT hot water system. Sol Energy 2017;158:285–94.

[33] Herrando M, Markides CN, Hellgardt K. A UK-based assessment of hybrid PV and solar-thermal systems for domestic heating and power: System performance. Appl Energy 2014;122(122):288–309.

[34] Fudholi A, Sopian K, Yazdi MH, Ruslan MH, Ibrahim A, Kazem HA. Performance analysis of photovoltaic thermal (PVT) water collectors. Energy Convers Manage 2014;78(1):641–51.